



HAL
open science

Plasma sputtering of biased electrodes in an oblique magnetic field

Paul Hiret, Kunal Soni, Anil Cherukulappurath Mana, E Faudot, Lucas Moser, Roland Steiner, Alessandro Geraldini, Stefano Alberti, Ivo Furno, Jérôme Moritz, et al.

► **To cite this version:**

Paul Hiret, Kunal Soni, Anil Cherukulappurath Mana, E Faudot, Lucas Moser, et al.. Plasma sputtering of biased electrodes in an oblique magnetic field. *Plasma Sources Science and Technology*, 2023, 32 (9), pp.095021. 10.1088/1361-6595/acfc63 . hal-04232910

HAL Id: hal-04232910

<https://hal.science/hal-04232910>

Submitted on 9 Oct 2023

HAL is a multi-disciplinary open access archive for the deposit and dissemination of scientific research documents, whether they are published or not. The documents may come from teaching and research institutions in France or abroad, or from public or private research centers.

L'archive ouverte pluridisciplinaire **HAL**, est destinée au dépôt et à la diffusion de documents scientifiques de niveau recherche, publiés ou non, émanant des établissements d'enseignement et de recherche français ou étrangers, des laboratoires publics ou privés.



Distributed under a Creative Commons Attribution 4.0 International License

PAPER • OPEN ACCESS

Plasma sputtering of biased electrodes in an oblique magnetic field

To cite this article: Paul Hiret *et al* 2023 *Plasma Sources Sci. Technol.* **32** 095021

View the [article online](#) for updates and enhancements.

You may also like

- [Kinetic plasma dynamics in a radial model of a Hall thruster with a curved magnetic field](#)
Alberto Marín-Cebrián, Adrián Domínguez-Vázquez, Pablo Fajardo et al.
- [Density polarization effect of spin-up and spin-down electrons on magnetosonic solitons in a dense plasma with oblique magnetic field](#)
S Hussain and S Mahmood
- [Improvement of photoresist etching by impedance control of a bias electrode in an inductive discharge](#)
You He, Yi-Lang Jiang, Jiwon Jung et al.



Analysis Solutions for your Plasma Research

- Knowledge
- Experience ■ Expertise

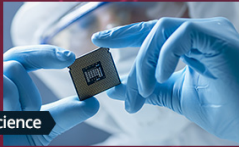
[Click to view our product catalogue](#)

Contact Hiden Analytical for further details:
W www.HidenAnalytical.com
E info@hiden.co.uk



Surface Science

- ▶ Surface Analysis
- ▶ SIMS



Surface Science

- ▶ 3D depth Profiling
- ▶ Nanometre depth resolution



Plasma Diagnostics

- ▶ Plasma characterisation
- ▶ Customised systems to suit plasma Configuration



Plasma Diagnostics

- ▶ Mass and energy analysis of plasma ions
- ▶ Characterisation of neutrals and radicals

Plasma sputtering of biased electrodes in an oblique magnetic field

Paul Hiret^{1,*} , Kunal Soni¹ , Anil Cherukulappurath Mana² , Eric Faudot²,
Lucas Moser³ , Roland Steiner¹ , Alessandro Geraldini⁴, Stefano Alberti⁴, Ivo Furno⁴ ,
Jérôme Moritz² , Frédéric Brochard² , Stéphane Heuraux², Laurent Marot¹ 
and Ernst Meyer¹ 

¹ Department of Physics, University of Basel, Klingelbergstrasse 82, CH-4056 Basel, Switzerland

² Institut Jean Lamour, UMR 7198 CNRS – Université de Lorraine, 2 allée André Guinier, BP 50840
54011 Nancy Cedex, France

³ ITER Organization, Route de Vinon-sur-Verdon—CS 90 046, 13067 St Paul Lez Durance Cedex, France

⁴ Swiss Plasma Center, Ecole Polytechnique Fédérale de Lausanne, route Cantonale, 1015 Écublens,
Switzerland

E-mail: paul.hiret@unibas.ch

Received 5 May 2023, revised 21 August 2023

Accepted for publication 22 September 2023

Published 3 October 2023



CrossMark

Abstract

The surface erosion of biased electrodes immersed in a radio frequency (RF) plasma was investigated in oblique magnetic fields ranging from 0.1 T to 3.5 T. The plasma potential and density in the vicinity of the biased electrode have been measured using an RF-compensated cylindrical Langmuir probe moved by a three-dimensional motorised arm in the ALINE facility at 0.1 T. The erosion profiles were determined for different gases (argon and helium), magnetic field strength and plasma volume for the same electrode surface area at an angle of 5° with the magnetic field in three different experimental geometries. The radial electric field (perpendicular to the magnetic field) in the plasma column has been deduced from plasma potential measurements. This radial field makes the ions converge to the core of the plasma column at grazing angles (<30°) and is reversed at larger angles. The ion flux on the sample increases with the magnetic field magnitude leading to a strong erosion inhomogeneity. At lower plasma volume, the erosion rate is sensitively enhanced. Local redeposition was identified using x-ray photoelectron spectroscopy on the surfaces exhibiting preferential deposition directions. Finally, the asymmetric erosion patterns obtained from a molybdenum layer etching are explained by the similar asymmetric density maps obtained with the probe and by the $\vec{E} \times \vec{B}$ drift and the local sheath acceleration.

Supplementary material for this article is available [online](#)

Keywords: RF plasma, erosion pattern, first mirrors, magnetised plasma, plasma-surface interactions, x-ray photoelectron spectroscopy

* Author to whom any correspondence should be addressed.



Original Content from this work may be used under the terms of the [Creative Commons Attribution 4.0 licence](#). Any further distribution of this work must maintain attribution to the author(s) and the title of the work, journal citation and DOI.

1. Introduction

Radio-frequency (RF) capacitively coupled plasma (CCP) is commonly used in industry and laboratory. Magnetic fields are used in various applications for controlling CCPs and improving the performance of etching processes in the semiconductor industry [1–5]. Moreover, a wide range of techniques requires the operation of CCPs in the presence of an external magnetic field, in particular in Hall effect thruster where plasma erosion of the discharge chamber's walls decreases the thruster lifetime [6–10]. Similar erosion behaviour on ion cyclotron resonance heating antennas has been reported in magnetic fusion devices [11–13]. RF sheaths develop in front of antennas, causing surface damage by ion sputtering and degrading their efficiency [14, 15]. In fusion devices, RF discharges are also foreseen for the cleaning of the first mirrors in optical diagnostics [16–18]. The first mirrors, being the front-end components in these diagnostic systems, are subjected to constant deposition from the first wall materials of the fusion reactor vessel, which significantly degrades their optical performance [19–22]. To recover optical efficiency, *in-situ* cleaning processes utilising RF CCP discharges are under development [23]. A few studies on plasma cleaning in a magnetic environment have already been performed [24–26].

In CCPs, the ion flux homogeneity toward the electrode influences the erosion profile. The presence of a magnetic field \vec{B} severely alters the kinetics of the ions and electrons in the plasma, which tend to gyrate around the \vec{B} field lines. Likewise, the strongly magnetised plasma particles follow the field line confining the plasma in a column of the electrode size. While the flux along the magnetic field lines is unaffected the transport of particles perpendicular to the magnetic field occurs mainly with collisions [27]. Additionally, in CCP discharge, the electrode acquires negative self-bias, leading to the formation of an electric field E_e in the sheath toward the electrode. Moreover, Chodura evidenced the formation of a neutral magnetic presheath scaling with the ion Larmor radius in front of the Debye sheath when the ion Larmor radius is larger than the Debye length [28]. The average ion incidence angle at the wall tends to be at the magnetic field angle while the magnetic field value increases [29]. The quasi-neutral magnetic presheath disappeared when the magnetic field was almost perpendicular to the surface. In these conditions, the ions enter the sheath along the magnetic field lines with Bohm velocity and reach the electrode surface with an average incidence angle similar to the magnetic field angle [30]. Kobelev *et al* demonstrated that the change in the inclination angle from normal to 5° to the surface was responsible for an increase by more than ten times of the average ion transit time in the sheath increasing the ion-neutral collisions number within the sheath leading to a broadening of the ion energy distribution function [31].

The influence of the magnetic field's magnitude and the angle between the electrode surface plane and the magnetic field on the self-bias voltage have already been reported [24, 25, 32] altering the sheath electric field. The presence of this crossed electromagnetic field induces an $\vec{E}_e \times \vec{B}$ drift

which affects the uniformity of the ion distribution on the surface. Yan *et al* noticed an inhomogeneity of the erosion on the surface being higher in the centre of the electrode [25], where the 1.77 T incident magnetic field was at an angle of 5° from the surface of the electrode. These observations were attributed to the local change of the incident ion flux.

Knowing plasma density and potential in the vicinity of the samples is necessary to understand the ion flux distribution toward the electrode's surface. However the presence of the magnetic field modified the particle kinetics and so the way they are collected by a cylindrical electrostatic probe aligned with the magnetic field. Under a magnetic field, orbital motion limit theory is valid for ions even in some RF discharges, but not for the electrons as part of the electrons reach the probe only by moving along the B -field [33]. Indeed, the saturated electron current is much lower in the magnetic field compared to the unmagnetised case due to the collapsing of the electron transport perpendicularly to the magnetic field [34]. Moreover, wrong estimation of the plasma parameters due to electron density depletion when the probe voltage was higher than the plasma potential has been reported [35]. Then, the plasma density can be deduced from the ion saturation part of the probe current–voltage characteristics with higher reliability than with the electron part in magnetised conditions considering quasi-neutrality of the plasma [36]. Measurements of plasma density and potential in the vicinity of a biased electrode in an oblique magnetic field reported by Ledig *et al* showed non-uniform radial profiles of the density and the plasma potential in the plasma column at 0.1 T when the ions are non-magnetised [36]. Furthermore, homogeneous electrode erosion in magnetised CCP discharges should not be possible for small incident angles of the magnetic field lines on the RF electrode [36].

With the purpose of efficient mirror cleaning in such magnetic environments, we have performed further investigations to improve our understanding of the inhomogeneous erosion patterns observed in the preceding studies. In this manuscript, we conducted an experimental characterisation of the plasma column using a Langmuir probe at 0.1 T. Then, we focused on the impact of the magnetic field intensity and the plasma column volume on the erosion profile on similar biased electrodes in different magnetised CCP devices. To have an angle between the mirror surface and magnetic field similar to what is expected in ITER, experiments were mainly performed at 5° .

2. Experimental

2.1. Samples

Plasma erosion experiments were performed using copper (Cu) electrodes. A 200 nm nanocrystalline molybdenum (Mo) layer, used as an erosion marker, was deposited on each electrode by magnetron sputtering [37]. The thickness of the Mo layer was quasi-homogeneous over the electrode surface ($\pm 15\%$) and was determined before and after

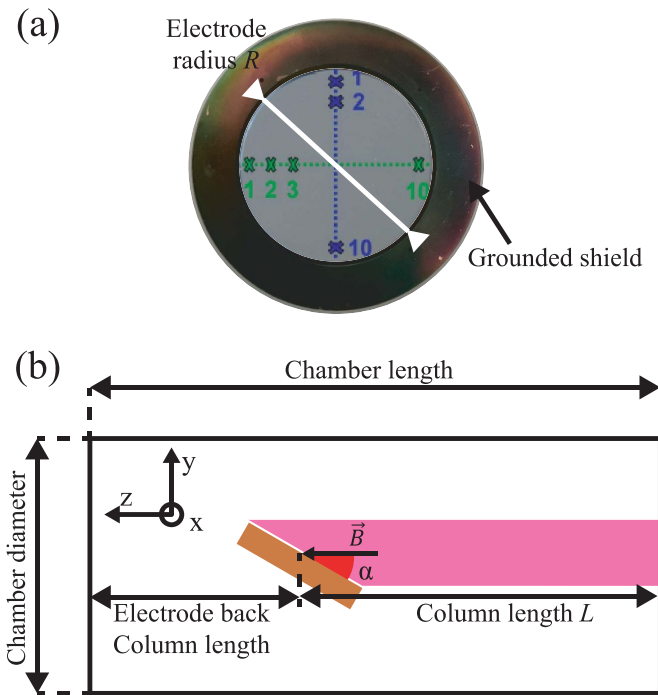


Figure 1. Picture of the electrode (a) and schematic of the setups (b).

each experiment using energy-dispersive x-ray spectroscopy (EDX). The thickness was measured from the centre of the electrode every 5 mm in the direction of \vec{B} and $\vec{E}_e \times \vec{B}$ (figure 1(a)). The EDX measurements were done on the Philips XL30 ESEM microscope, varying the acceleration voltage from 3 to 30 kV. The fitting of the EDX data was performed using STRATAGEM software and is described in detail elsewhere [38]. The surface chemical composition of the samples was characterised using x-ray photoelectron spectroscopy (XPS). The XPS measurements were carried out using a VG ESCALAB 210 spectrometer using monochromatised Al $K\alpha$ radiation (1486.6 eV) and with an energy resolution greater than 0.5 eV [39].

2.2. Experimental setups

Depending on the size of the grounded vacuum chamber in comparison to the electrode and of the magnetic field required for the experiments, three experimental facilities described in the following were used.

2.2.1. ALINE: 0.1 T. The first facility is ALINE (A LINEar plasma device). It operates at low magnetic fields (0 to 0.1 T maximum) thanks to six circular coils equally distributed along the 1000 mm long and 300 mm diameter of the cylindrical chamber. The magnetic field strength is perfectly homogeneous in the whole discharge chamber. At 1 Pa and 0.1 T, the ions are unmagnetised [35]. The rotatable electrode was mounted at the centre of the chamber and allowed the performing of experiments at various angles α with respect to the magnetic field lines (figure 2). The cathode was a 48 mm

diameter copper disk driven at 25 MHz and surrounded by a grounded copper shield. The plasma parameters (density, temperature, floating and plasma potentials) were measured with a movable RF-compensated Langmuir probe in helium (He) and argon (Ar) discharges. The tungsten tip (10 mm long and 0.075 mm radius) of the probe was mounted on a motorised three-axis manipulator, which allows obtaining 3D density maps of the explored plasma [36, 40]. The tungsten tip was parallel to the magnetic field. All the measurements were performed in the XY plane at $z = -180$ mm (meaning 180 mm away from the cathode, as shown in figure A1), where the density disturbance caused by the probe was minimum.

2.2.2. Basel University Magnetised Plasma facility (BUMP): 0.5 T. BUMP procured the smallest grounded vacuum chamber. The background pressure in the vessel was around 10^{-4} Pa. The 100 mm long and 200 mm wide chamber is installed between two water-cooled coils of an electromagnet Bruker B-E 15 powered by a Bruker B-MN90 power unit (as shown in figure A2(a)). By varying the current, the magnetic field inside the chamber can be increased up to 0.58 T. The field homogeneity at this magnitude is presented in figure A2(b). The magnetic field varies by 10% in the chamber but only by 3% around the electrode. This electrode was centred in the vacuum chamber and could rotate to vary the angle α between the surface and the magnetic field (figure A2). Two models of electrodes were used: (i) a 50 mm diameter circular electrode similar to the one used in ALINE (ii) a rectangular electrode (30×49 mm²). The latter was shifted to 40 mm from the chamber's centre, allowing the positioning of a grounded counter-electrode parallel to the antenna, as shown in figure A2(d). The CCP discharges were driven by a 60 MHz RF generator.

2.2.3. LAusanne Magnetised Plasma facility (LAMP): 3.5 T. Erosion experiments up to 3.5 T were performed in the LAMP [24]. It includes a cylindrical vacuum chamber that was 453 mm long and 125 mm wide. The background pressure in the vessel was around 10^{-4} Pa. The superconducting magnet is composed of two coils cooled by liquid helium, producing a magnetic field up to 3.5 T in the centre with a variation of 3% in the vicinity of the electrode. The magnetic field is regulated by the current, and its polarity can be reversed. The distribution of the magnetic field is Gaussian (figure A3), with a maximum at the electrode. The electrode had a diameter of 48 mm and was surrounded by a grounded shield. The rotation of the electrode allowed the investigation of different angles α with the magnetic field. Argon was used for the discharges with a pressure of 1 Pa. The CCP discharges were driven by a 60 MHz RF generator.

3. Results and discussion

3.1. Plasma density in the vicinity of the electrode

As explained in the introduction, magnetised charged particles follow and gyrate around the magnetic field lines, confining

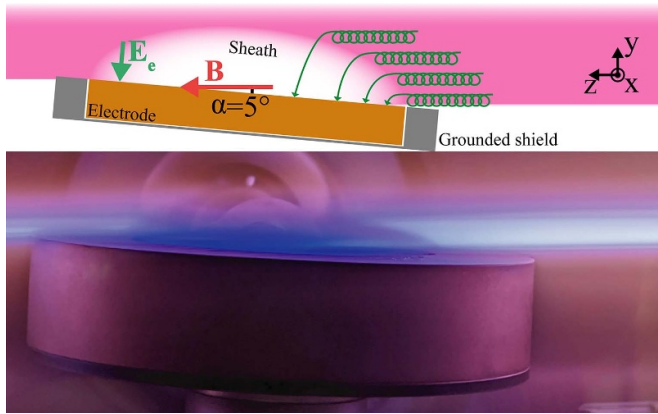


Figure 2. Picture of plasma column in the vicinity of the electrode. The electrode surface was at an angle of 5° with respect to the magnetic field. Possible ions trajectories are drawn in green.

the plasma in a column connected to the electrode. Actually, the plasma column is as large as the plasma sheath (figure 2), which can be seen just above the surface of the electrode, where the brightness is lower because of the low electron density. The sheath is responsible for stochastic heating in magnetic field [41]. At grazing angles ($\alpha < 5^\circ$), the thickness of the sheath allows the plasma to expand on both sides of the electrode because the projected vertical shield width is smaller than that of the sheath. In contrast, at larger angles, the plasma column extends only on one side of the electrode because the shield entirely shadows the other side, as shown in figure S3.

In figure 3, radial plasma density maps near the electrode are displayed for two different gases: Ar and He. The centre of the electrode is located at $(x,y) = (0,0)$ mm. As the electrode is circular, the projection of the electrode in the direction of \vec{B} is an ellipse, and therefore the radial shape of the plasma column is the same. Its centre is shifted in the positive y -direction (figure 3). That was due to the shift of the plasma column to the sheath entrance (figure 2). The ions coming from the plasma column are accelerated at the entrance of the sheath towards the cathode, which is negatively self-biased (-100 V). The ion density is maximum at $6.2 \times 10^{16} \text{ m}^{-3}$ for He and at $2.0 \times 10^{17} \text{ m}^{-3}$ for Ar in the centre of the plasma column. The higher density in Ar discharge is coherent with the higher ionisation rate of Ar than for He for the same discharge voltage [42]. The fact that helium is ten times lighter results in a lower electron density than in argon plasma. The centre of the column was shifted due to the vertical sheath thickness of 10 mm in the y -direction for He and of 5 mm for Ar. As the sheath thickness is inversely proportional to the square root of the plasma density [27], the sheath was larger in the He plasma and then the plasma column centre was shifted more in the y -direction. The density decreased by a factor of 2.3 for He and of 3.4 for Ar within 10 mm in the positive y -direction (figure 3). In both discharges, the distribution of the density in the plasma column is slightly asymmetric. The reason for this asymmetry is discussed at the end of this section. The higher density in the core of the plasma column implied that most of the ion flux at the cathode was located on

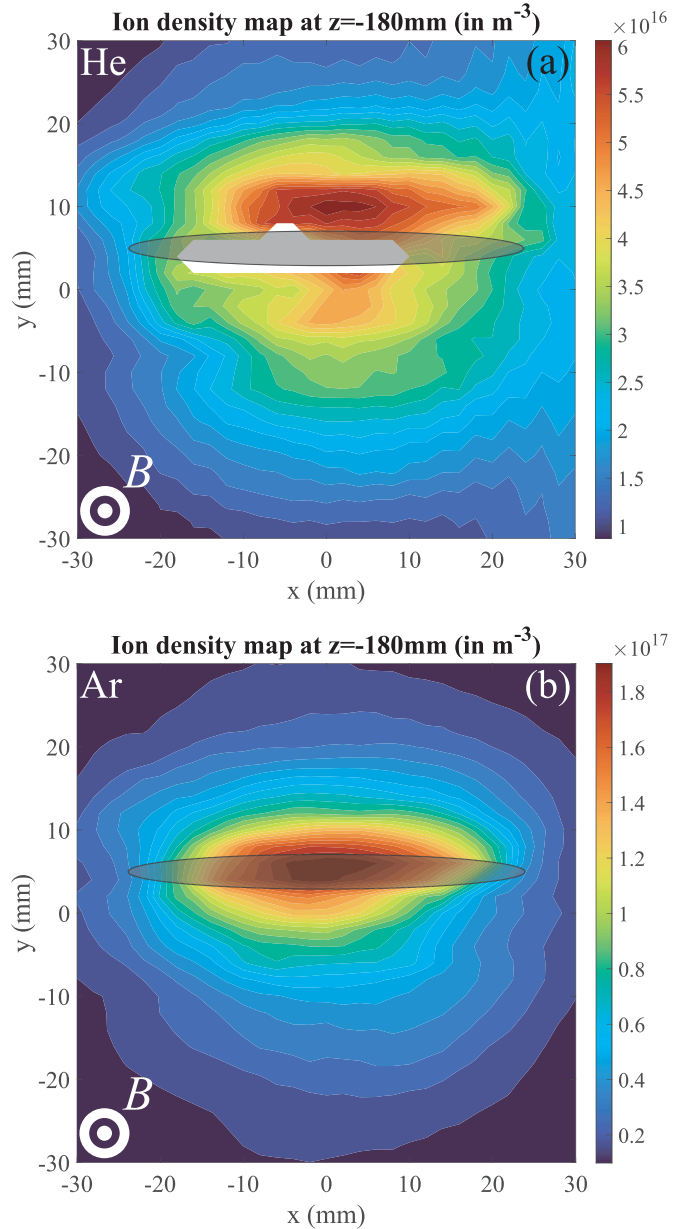


Figure 3. ALINE ion density maps measured in the plasma column in the x - y plane shown 180 mm far from the cathode in (a) helium and (b) argon discharge. The electrode was tilted at $\alpha = 5^\circ$. In the white area of (a) the measurements were not consistent.

the front edge of the electrode, as shown in figure 2. At the top of the sheath, the ion density must be lower and thus the ion flux towards the cathode mainly in the central part is lower.

At grazing angles with helium, the plasma potential V_p was maximum at 22 V in the outer part of the bright plasma column and decreased to 10 V in the core, as shown in figure 4(a). In helium discharges, a higher potential (22 V) column was measured in the centre of the potential map. This inhomogeneity generates a stationary averaged radial electric field \vec{E}_c directed toward the centre of the plasma column with values given in table 1. This electric field was responsible for confining the unmagnetised ions in the core of the plasma beam leading to a higher density in the plasma column core, as observed in

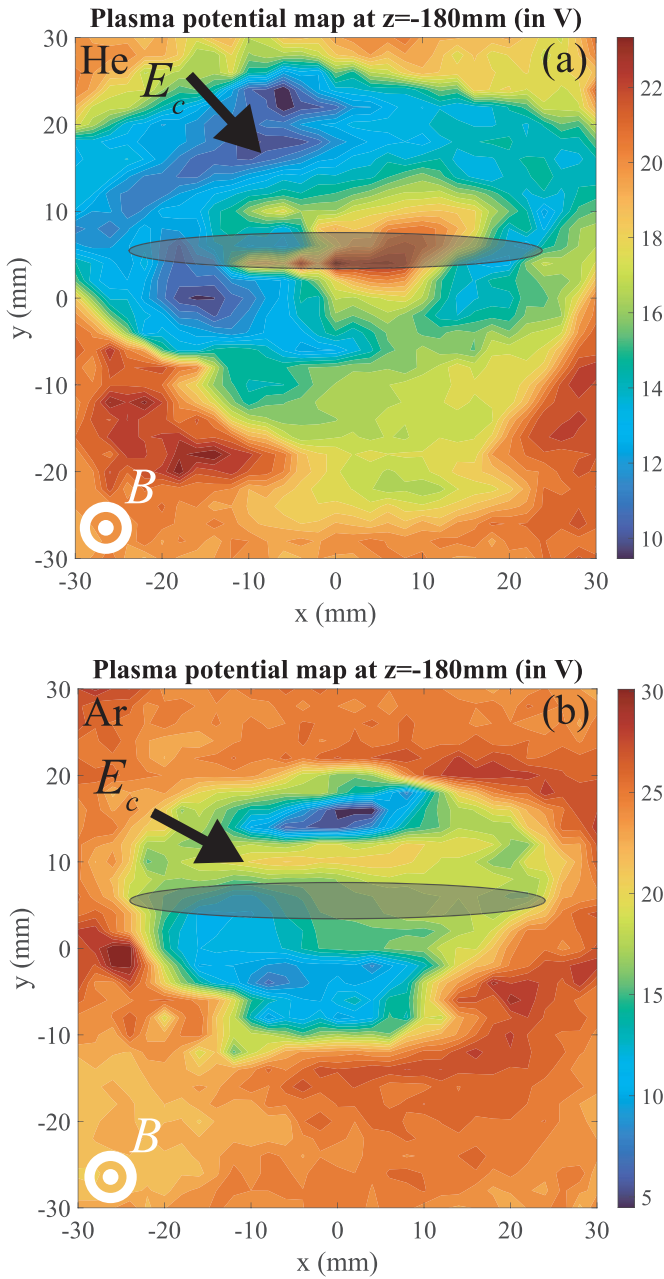


Figure 4. ALINE plasma potential maps measured in the plasma column in the plane xy shown 180 mm far from the cathode in for a CCP plasma with (a) helium and (b) argon. The electrode was tilted at $\alpha = 5^\circ$.

figure 3. In addition, the charged particles are subject to an $\vec{E}_c \times \vec{B}$ drifts directed in the azimuthal direction, as shown in figure 5. At a low B field (0.1 T), electrons follow this $\vec{E}_c \times \vec{B}$ drift, leading to a net electron current flowing around the plasma column. This additional electron velocity in the azimuthal direction slightly increases the ionisation and, consequently the plasma density. The typical magnitudes of these drifts have been calculated in table 1. Another drift is due to the radial density gradient in the plasma column. As shown in figure 4, the density at the edge of the column is roughly 3 times lower than that at the centre. Because ions are still

Table 1. Table of magnitude inside the plasma column at 0.1 T with $\alpha = 5^\circ$.

	He	Ar
V_p in the core ($r = 0$ mm) (V)	14	20
V_p in the periphery ($r = 20$ mm) (V)	22	26
Radial E_c field (V.m^{-1})	-4×10^2	-3×10^2
$E_c \times B$ field (m.s^{-1})	4×10^3	3×10^3
Diamagnetic drifts v_{De} (m.s^{-1})	3×10^3	3×10^3
Global drift (m.s^{-1})	7×10^3	6×10^3

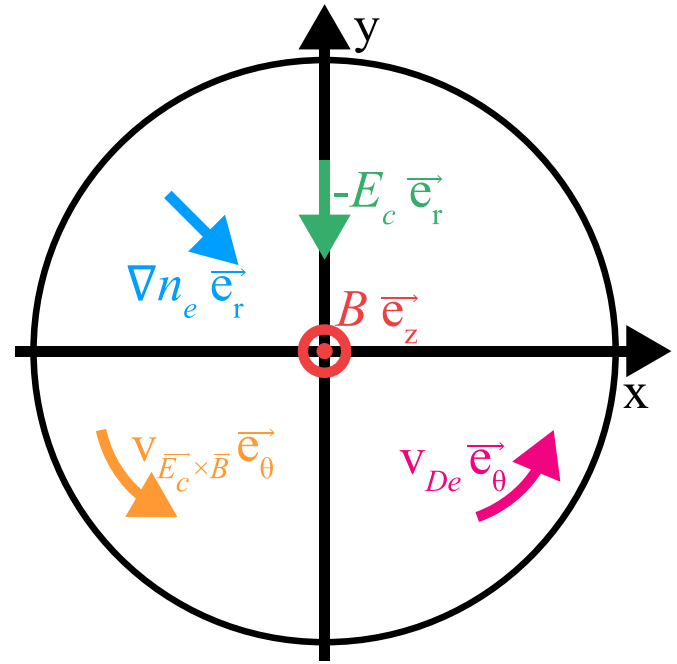


Figure 5. Schematic of the drifts occurring in a cylindrical plasma column referring to table 1.

considered as unmagnetised at $B = 0.1$ T, only the magnetised electron contributes to the diamagnetic drift, resulting in a net azimuthal electron current known as the diamagnetic current. This diamagnetic drift created by a non-uniform electron density n_e in a magnetic field is given by [43]:

$$\vec{v}_{De} = \frac{T_e \vec{\nabla} n_e \times \vec{B}}{q n_e B^2} \quad (1)$$

where T_e the electron temperature is assumed to be constant in the plasma column, and q is the elementary charge. The electron temperature was quasi-homogeneous in the plasma column at 3 eV. According to the electric field direction in figure 3, both $\vec{E}_c \times \vec{B}$ and diamagnetic drifts are in the same direction contributing to a larger global drift around the plasma column (figure 5).

At $\alpha = 30^\circ$, ions are well confined in the plasma column connected to the electrode due to the convergent radial electric field (see figure S2(a)). To respect the quasineutrality, the sheath potential self-consistently increases to repel more electrons and increase the electron density in the same way as for ions. Consequently, the density map (figure S2(b)) exhibits

a higher value in the central region, where a higher erosion rate can be expected. At $\alpha = 45^\circ$, the radial electric field is reversed (figure S3(a)), ions are expelled out of the centre of the plasma column (and electrons as well to maintain the quasineutrality), resulting in a lower density in the central part and a higher one in the surroundings close the edge of the electrode. Again, the erosion pattern should be similar to the density map (figure S3b). At $\alpha = 45^\circ$, the $\vec{E}_e \times \vec{B}$ drift was directed in the negative azimuthal direction and was then opposite to the diamagnetic drift. Both drifts can cancel each other by applying a well-chosen electric field, as shown in [44, 45].

The previous drifts ($\vec{E}_e \times \vec{B}$ and diamagnetic drifts) occur in the quasi-neutral plasma. But inside the RF sheath, the averaged electric field \vec{E}_e can be as high as $1.2 \times 10^4 \text{ V.m}^{-1}$ (-120 V over the 10 mm sheath thickness) towards the electrode surface. The $\vec{E}_e \times \vec{B}$ drift can thus be as high as $1.2 \times 10^5 \text{ m.s}^{-1}$ for electrons at 0.1 T , which is the order of the typical thermal velocity for several electron-volts (roughly $7 \times 10^5 \text{ m.s}^{-1}$ at 3 eV). It implies a strong cross flux of electrons over the electrode, displacing the density over the surface of the electrode depending on the direction of the magnetic field.

According to Poisson's equation, the potential in the sheath obeys a parabolic law resulting in a linear electric field which was maximum at the surface of the electrode and minimum at the entrance of the sheath. On the contrary, the electron density follows an exponential profile and consequently is maximum at the entrance of the sheath and close to zero at the surface of the electrode. The resultant electron flux is the product of both density and drift velocity proportional to the electric field and is then maximum close to the surface of the electrode. At 0.5 T , the drift velocity is roughly 35 times smaller than the thermal velocity. At 3 T , the effect of the $\vec{E}_e \times \vec{B}$ drift could be neglected.

Finally, all these drifts at low electrode angles led to the asymmetric shape of the plasma density in the x -direction in figure 2. Part of the density was drifted from the left side to the right side above the shielded electrode. Reversing the magnetic field results in the same opposite shape in the x -direction. For higher magnitudes of \vec{B} , the global drift velocity is negligible compared to the thermal velocity reducing the asymmetry of the plasma column.

3.2. Influence of the magnetic field strength on the erosion profiles

Erosion experiments were carried out in LAMP using Ar plasma at $\alpha = 5^\circ$ for $0, 0.1, 0.5$ and 3 T . The self-bias developed on the electrode depends on the RF power and the magnitude of the magnetic field [26]. To keep the self-bias constant at -100 V , the RF power was varied accordingly to the different magnetic field values. The corresponding parameters are presented in table 2. The ratio of the ion cyclotron frequency ω_{ci} to the ion plasma frequency ω_{pi} is given as an indication. Total erosion of the Mo layer on part of the electrode was used as an indicator to stop the exposure. Given the Mo thickness was nearly homogeneous, and the self-bias was

Table 2. Table displaying the RF power and exposure time for the erosion experiments in Ar discharges at different magnitudes of \vec{B} and a constant self-bias of -100 V . The sample was tilted at $\alpha = 5^\circ$.

Field value (T)	Power (W)	Exposure time (min)	ω_{ci}/ω_{pi}
0	25	190	—
0.1	35	90	0.003
0.5	40	28	0.02
3	75	21	0.09

constant, the erosion profile visually changed with the magnetic field value (figure 6). At 0 T , there was no visual change observed on the sample, as shown in figure 6. The erosion rates were similar in both \vec{B} and $\vec{E}_e \times \vec{B}$ directions at roughly $3 \times 10^{-2} \text{ nm min}^{-1}$. The erosion was homogeneous along the electrode except at the edges (figure 7), where the erosion rate increased to $1.6 \times 10^{-1} \text{ nm min}^{-1}$. The stronger erosion at the edges is due to higher ion fluxes on the perimeter of the electrode. This is due to the addition of E -field lines from the grounded shielding around the sample. In the direction of \vec{B} , the peak erosion rate was enhanced by 450 times at 3 T in comparison to that obtained at 0 T (figure 7(a)). At 0.1 T and 0.5 T , the peak erosion rates increased by 120 and 375 times, respectively, when compared to 0 T . At 0 T and 0.1 T , ions are not magnetised and then the average incident angle on the surface is almost 90° (figure 8). For this incident angle, the sputtering yield is approximately $0.2 \text{ atoms.ion}^{-1}$ for an incident energy of 130 eV [46]. Whereas at 0.5 T and 3 T , the IADF was typically centred at lower angles and broadened [29, 31, 47]. With an incident energy of 130 eV , the sputtering yield is increasing quasi-linearly from 0.2 with an incident angle to the surface plane of 90° to a maximum of $0.45 \text{ atoms.ion}^{-1}$ at 35° (figure S4) [48,49]. The sputtering yield is then a maximum of 2.3 times larger than at 90° . While the measured erosion rates were 3.2 times higher at 0.5 T than at 0.1 T . In these conditions, the higher observed erosion rate was not only caused by an increase of the sputtering yield due to the change of ion incident angle but also by an increase of the ion flux or the ion energy which are related to an increase of the density or electron temperature in the vicinity of the electrode and to an increase of the plasma potential (self-bias was set constant at -100 V) respectively. The increase of the required power to maintain a -100 V electrode self-bias led to an increase of either the ion flux or the ion energy with the magnetic field.

The erosion rate on the surface of the electrodes in the directions of $\vec{E}_e \times \vec{B}$ and \vec{B} at different field magnitudes are presented in figure 7. As shown in figure 6, the Mo layer was completely eroded in the lower part of the electrode. Therefore it was not possible to measure the erosion rate at this location, at these points, a projected erosion rate was calculated based on the trend. As indicated in figure 7(b), there was an erosion peak between -2.5 and 2.5 mm (close to the centre of the electrode) in the direction of $\vec{E}_e \times \vec{B}$ at 3 T with a peak erosion rate of 13 nm min^{-1} . This peak in the erosion profile in the

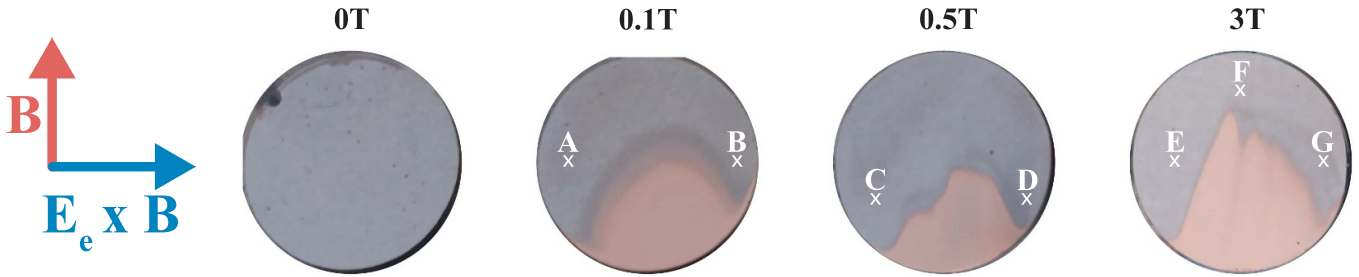


Figure 6. Erosion of the molybdenum layer on a copper cathode biased at -100 V immersed in plasma with an angle $\alpha = 5^\circ$ for different magnetic fields: 0, 0.1, 0.5, 3 T (left to right).

(Note: The plasma exposure times and power applied for the samples were different.)

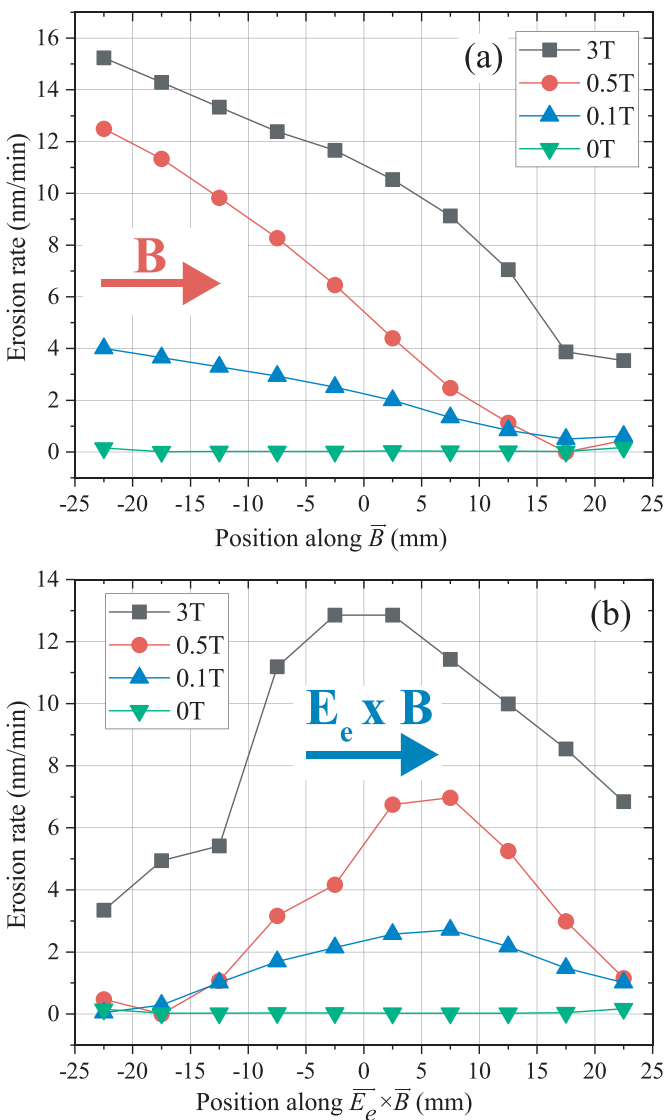


Figure 7. Comparison of the erosion rates for different \vec{B} magnitudes in the direction of (a) \vec{B} and (b) $\vec{E}_e \times \vec{B}$ for electrode an angle $\alpha = 5^\circ$.

direction of $\vec{E}_e \times \vec{B}$ drift was also observed at lower magnetic fields. Furthermore, the peak was shifted in the direction of positive $\vec{E}_e \times \vec{B}$ for a lower magnetic field (at $+7.5$ mm for 0.1 T). This erosion peak results from an increased ion

density in the direction of $\vec{E}_e \times \vec{B}$. At 0 T, the erosion rates were identical in both x - and y -directions except for the edges, where the erosion rate is higher. This is a result of a higher ion flux on the electrode's perimeter, which arose from the E -field between the grounded shielding around the sample and the biased electrode [50]. The erosion profile in a B field can be understood following the results of section 3.1. The plasma potential inhomogeneity (figure 2) induced a higher ion density in the centre of the plasma column. In addition, the non-uniformity of the sheath thickness across the surface of the electrode led to a deviation of the ions at the entrance of the sheath (figure 4). Therefore the ion flux was higher on the portion of the electrode closer to the plasma beam.

On the electrodes exposed at 0.1 and 0.5 T, Cu was detected over the Mo layer on both sides of the 'V' erosion pattern via XPS measurements (figure 6, points A, B, C and D). On the contrary, at 3 T, no Cu was found in the direction of negative $\vec{E}_e \times \vec{B}$ (figure 6, point E). The Cu detected over Mo is essentially redeposited upon getting sputtered from the centre of the electrode. A similar local redeposition profile was reported for an experiment in a fusion reactor (DIII-D) in the area handling the heat fluxes [51] where a Mo target surrounded by a graphite ring was exposed to the plasma with a toroidal \vec{B} of 2.3 T. The graphite ring analysed by Rutherford back-scattering displayed net redeposition of Mo all around the target. However in the positive directions of \vec{B} and in the $\vec{E}_e \times \vec{B}$, the Mo deposition was about an order of magnitude higher than on the other sides, indicating higher transport along the direction of the magnetic field. Three main mechanisms of redeposition were identified to occur in a magnetic field: (i) prompt redeposition can occur when the sputtered particle gets ionised and gyrate around the magnetic field lines [52], (ii) the parallel force due to the electric field in the sheath and in the magnetic pre-sheath transporting the ionised impurities back to the target [53], (iii) momentum transfer from the ion beam to the sputtered atoms. The particle deposition direction depends principally on the angle of the sputtered particles and therefore on the angle of incidence of the ions to the surface. At 0.1 T, the ions were not magnetised therefore the expected mean value of the IADF was almost normal to the surface (figure 8). For this field strength, the ionised sputtered particles do not gyrate in the length scale of the electrode and therefore did not participate in prompt redeposition. Therefore at 0.1 T and lower, redeposition was only due to momentum transfer

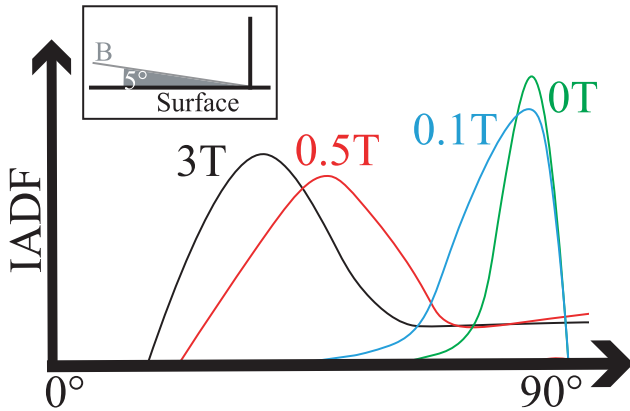


Figure 8. Schematic of the ion angular distribution function for different B -field magnitude tilted from 5° to the electrode surface.

and parallel force deposition. Thus, the angular distribution of the sputtered species ejected from the surface can typically be approximated by a cosine distribution and get redeposited everywhere on the sample. At 0.5 T, the particle strikes the surface with a lower angle than at 0.1 T. The Larmor radius of the plasma ions (≈ 2 mm for Ar considering $T_i = T_e = 3$ eV) was also responsible for a broadening of the IADF and for a farther transport of sputtered ionised particles on the sample along the positive and the negative $\vec{E}_e \times \vec{B}$ directions. At this field magnitude, the Cu ion gyrated with a radius of roughly 2 mm, which was an order lower than the electrode size allowing prompt deposition to occur in addition to other redeposition processes. At 3 T, the IADF was typically centred around lower angle than at 0.5 T and 0.1 T, the copper atoms were then sputtered in preferential directions which were along the positive \vec{B} and $\vec{E}_e \times \vec{B}$ [54].

3.3. Geometrical parameters

3.3.1. Influence of the plasma volume on the erosion rate.

Erosion experiments were conducted in LAMP with different orientations of \vec{B} and plasma volumes at 13.56 MHz with a constant self-bias of -200 V. At 3.5 T and $\alpha = 5^\circ$, the plasma is confined in a column with a volume $V = L\pi R^2 \sin \alpha$ where R is the radius of the electrode, and L the distance parallel to the B field between the wall and the centre of the electrode (figure 9). As the electrode was not centred in the vertical direction of the chamber, the magnetised plasma volume could be changed by simply changing the orientation of the electrode from $\alpha = 5^\circ$ to $\alpha = -5^\circ$ as shown in figure 9. The input power was 8 W for $\alpha = 5^\circ$ and 21 W for $\alpha = -5^\circ$. The erosion rate measured in LAMP on the front edge of the electrode was 2.5 times higher for the configuration figure 9(b) than in the configuration figure 9(a). The erosion rate on the front edge of the electrode was enhanced with the same rate as the power, which was 2.6 times higher in configuration (b) than (a). The length and so the volume of the plasma column was reduced by a factor 5.2 from configuration (a) to (b). On the other hand, the erosion in the centre of the electrode was similar for

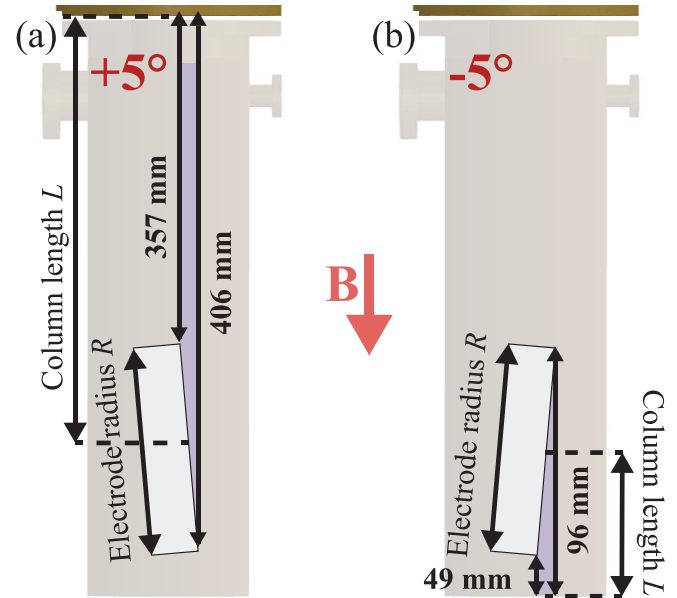


Figure 9. Schematic of varying plasma column volume in LAMP for (a) $\alpha = 5^\circ$ and (b) $\alpha = -5^\circ$. The distances to the ground are indicated.

both configurations (≈ 10 nm.min $^{-1}$). Similarly, the maximum erosion rate in the $\vec{E}_e \times \vec{B}$ was enhanced by 2.1, while in the electrode centre, the erosion rate was similar. The inhomogeneity of the erosion in the direction of both \vec{B} and $\vec{E}_e \times \vec{B}$ increased when the plasma column length and so volume were reduced. The enhanced erosion rate measured on the electrode can be due to an increase in the plasma potential, and then in the ion temperature. The plasma volume occupied by the sheaths in configuration 9b is much larger in proportion, and ions are mainly accelerated (heated) inside the sheath, which could explain a global higher ion temperature. In addition, the higher power required to maintain a self-bias of -100 V on the electrode while reducing the column length may be due to a sensitive increase in the density in the plasma column. As shown in the schematic figure 9, at $\alpha = 5^\circ$, \vec{B} was directed from the grounded wall to the electrode whereas at $\alpha = -5^\circ$, \vec{B} pointed from the electrode to the plasma wetted area. The influence of a reversed \vec{B} field was investigated at $\alpha = 5^\circ$ by reversing the direction of the \vec{B} (in grey in figure 10). In the x -direction in figure 10(a), the erosion profiles at $\alpha = 5^\circ$ were not influenced by the B field direction. However, when the magnetic field or the electric field ($\alpha = -5^\circ$) were inverted, the $\vec{E}_e \times \vec{B}$ and hence the erosion profile was mirrored. The higher erosion rate at $\alpha = -5^\circ$ indicated a higher ion flux toward the electrode and, therefore, larger ion density in the plasma column near the cathode, which is corroborated by the increase of the RF power.

3.3.2. Influence of setup geometry on the erosion rate.

Three samples were exposed to a magnetised plasma at 0.1 T with $\alpha = 5^\circ$ in the three different setups and the erosion

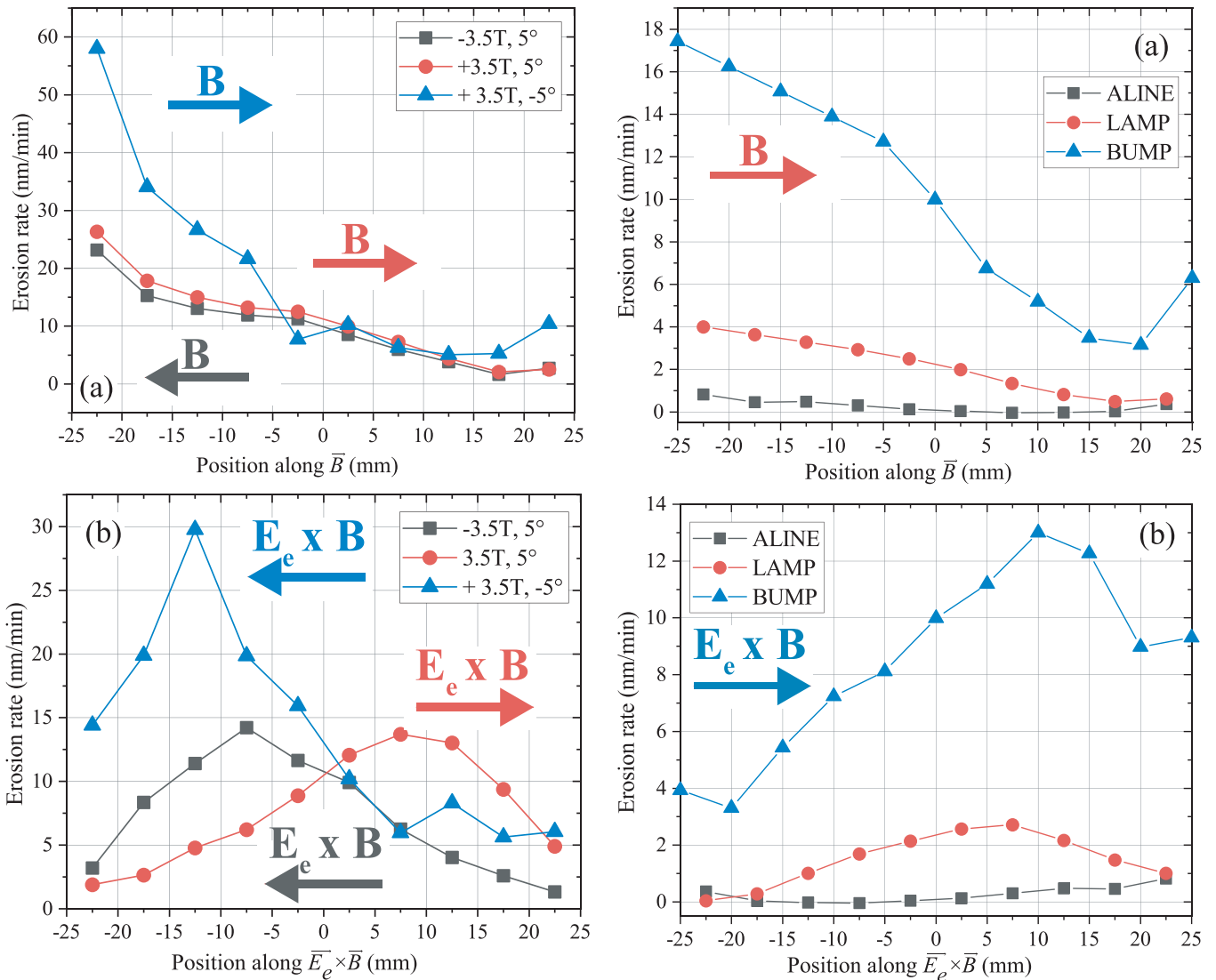


Figure 10. Comparison of the erosion rates for different directions of magnetic field and angles along (a) \vec{B} and (b) $\vec{E}_e \times \vec{B}$.

profiles measured were compared in figure 11. The sample self-bias was kept constant at -100 V during the erosion process. The power was set to keep the same self-bias in the different setups. The exposure time was adjusted with the setups to have noticeable erosion on the samples. The first sample was exposed for 270 min in ALINE with a power of 20 W. The second was exposed to plasma in the LAMP facility (configuration figure 9(a)) for 90 min at 35 W. Finally, the third was exposed in BUMP for 20 min with a power of 78 W. The RF frequency was 60 MHz in BUMP and LAMP and 25 MHz in ALINE. The erosion profiles in both \vec{B} and $\vec{E}_e \times \vec{B}$ directions were similar in BUMP and LAMP, showing a visible V-shaped erosion (as shown in figure 11(c)). However, the maximum erosion rate was 3.5 times higher in BUMP than in LAMP, while the plasma column was 11.7 times smaller than in LAMP (in BUMP, the centre of the electrode is located at 40 mm from the wall). Similar results were observed in LAMP while reducing the plasma column volume, as observed in section 3.3.1. The erosion in the front edge in the direction

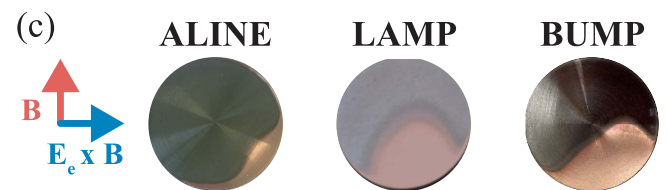


Figure 11. Comparison of the erosion rates for different setups at 0.1 T in the direction of (a) \vec{B} and (b) $\vec{E}_e \times \vec{B}$.

of \vec{B} in BUMP was 1.8 times larger than in the centre of the electrode, while this ratio was 1.7 in LAMP. Despite the enhanced erosion in BUMP, the distribution of the erosion rate over the electrode in the direction of \vec{B} is similar in LAMP and in BUMP. Regarding the erosion of the electrode in ALINE, in the direction of \vec{B} , the maximum erosion rate measured was 4 times lower than in LAMP. In contrast, the volume of the plasma column in front of the electrode was at least 1.3 times lower in LAMP than in ALINE. Moreover, the plasma was expanding in both directions from the electrode, and the plasma column in the electrode backside was longer in ALINE (≈ 450 mm) than in LAMP (≈ 49 mm) and so the

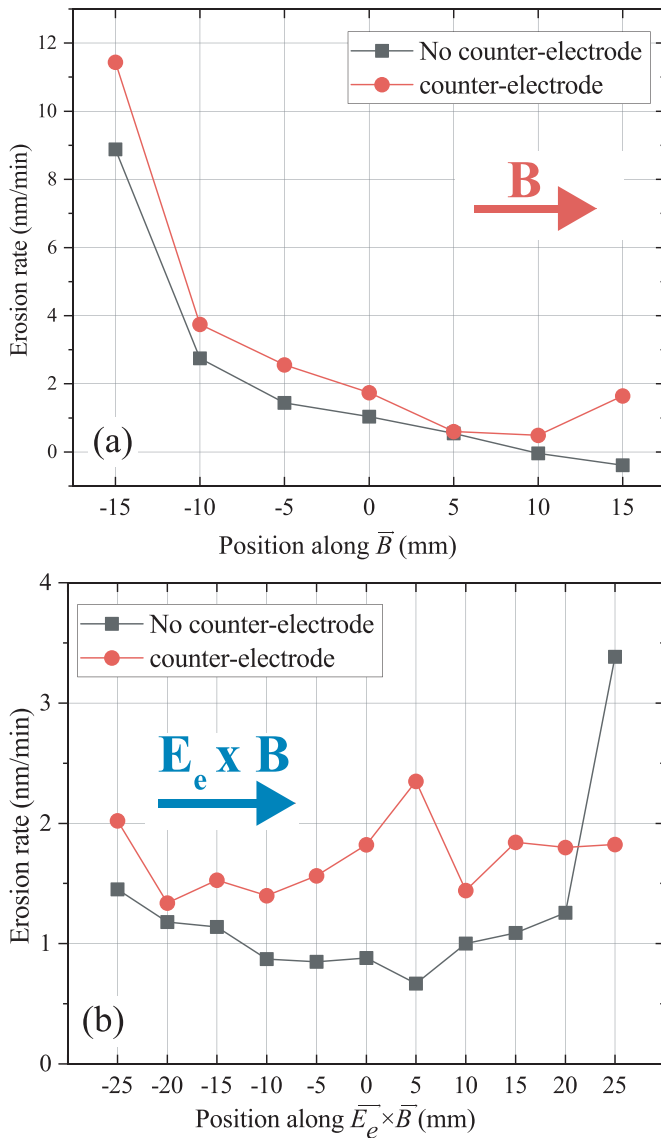


Figure 12. Comparison of the erosion rates with and without counter-electrode in the direction of (a) \vec{B} and (b) $\vec{E}_e \times \vec{B}$ at $\alpha = 10^\circ$.

plasma volume was much larger in ALINE. The length of the plasma column was linearly proportional to the volume and the electrode radius was the same in ALINE and LAMP. The erosion rate was enhanced in LAMP and in BUMP while the plasma column length and so volume were smaller. For a smaller column length L , more power is required to keep -100 V self-bias and may be related to an increase of the plasma density. Similar results were observed in LAMP while reducing the plasma column length, as observed in section 3.3.1.

3.3.3. Influence of a uniform connection length on the erosion rate. In the previous sections, the electrodes were tilted while the grounded walls in front were always perpendicular to the B field. That led to an unequal distribution of the distance between the electrode and the grounded wall over the

electrode surface. That distance is called the connection length from the electrode to the wall. Experiments were carried out in BUMP using a tilted counter-electrode in front of the rectangular sample (30×49 mm²) to equalise the connection length (figure A2). The average connection length at 10° was roughly 60 mm without the counter-electrode, whereas the connection length was 46 mm with the counter-electrode. The erosion profiles with and without counter-electrode were measured at $\alpha = 10^\circ$ (figure 12) and at $\alpha = 45^\circ$ (figure S4) in magnetic field of 0.5 T. It appeared in section 3.3.2, that increasing the average connection length (plasma column length) led to an enhanced erosion rate. Moreover, the connection length was smaller on the front edge (where the erosion rate was the highest) of the electrode than on the back edge (where the erosion rate was minimum) in the \vec{B} direction. One can expect that equalising the connection length over the electrode could have led to a homogenisation of the erosion rate over the electrode surface in the direction of \vec{B} . However, the erosion profile in both \vec{B} and $\vec{E}_e \times \vec{B}$ directions did not reveal noticeable differences when the connection length was equalised. The sheath developing around the electrode was concentrating the ion flux on the front edge of the electrode leading to a higher erosion rate in the electrode's front edge as discussed in section 3.1. Equalising the connection length did not modify the shape of the sheath in front of the electrode and so did not improve the homogeneity of the erosion rate along the \vec{B} field.

At $\alpha = 45^\circ$ the erosion profiles were homogenised along the B field direction, and the erosion rates were below 2 nm.min⁻¹ all along the direction of \vec{B} . However, further investigations on the shape of the electrode are required to understand the absence of a peaked erosion profile in the direction of $\vec{E}_e \times \vec{B}$ (figure 12(b)).

4. Conclusion and outlook

In the aim of studying the best way to clean the mirrors used in optical diagnostics in magnetic fusion machines, the sputtering of an RF-biased electrode has been investigated in a magnetised plasma. The ion density distribution in the vicinity of the electrode has also been studied to better understand the erosion distribution all over the electrode. The experiments were conducted in argon and helium discharges using an electrode at a tilt angle of 5° with the magnetic field direction. Three different experimental setups have been operated at 0, 0.1, 0.5 and 3.5 T.

The main results are summarised as follows:

The plasma potential maps measured in the plasma column at 0.1 T revealed an inhomogeneous potential inducing a radial electric field concentrating the ions inside the core of the plasma column as corroborated by the density measurements. The non-uniform distribution of the sheath layer around the electrode explains the deviation of the incoming ion flux close to the front edge of the electrode, while only a few fractions of this flux impinge the rest of the electrode surface. This has been confirmed by very inhomogeneous erosion rate profiles measured along the magnetic field direction. In addition, the

$\vec{E}_e \times \vec{B}$ drift showed a direct influence on the erosion profiles perpendicular to the magnetic field. The peak of the erosion rate drifted in the $\vec{E}_e \times \vec{B}$ direction, especially at low magnetic fields (0.1 T).

This erosion rate increased by a factor of 3.5 when the magnetic field increased from 0.1 to 3 T for constant self-bias of the electrode due to the strong magnetisation of the ions, which increased the plasma density and then the impinging flux on the electrode.

In the same way, a higher erosion rate has been measured for lower plasma volume (lower connection length) at 3.5 T and suggested a higher ion flux for a shorter plasma length. Finally, the setup of a grounded counter-electrode (to maintain the connection length constant between both electrodes) did not improve the homogeneity of the erosion profile.

The experiments presented here provide important results on ion-surface interaction in an oblique magnetic field. The plasma density and the erosion rate measurements indicate that homogeneous etching of a tilted circular surface in magnetised plasma cannot be achieved for grazing angles due to $\vec{E}_e \times \vec{B}$ drift and inhomogeneous plasma density over the electrode. Such inhomogeneous erosion in grazing magnetic fields may prevent the active cleaning of first mirrors in the next-generation fusion devices.

However, different mirror geometries could be investigated to mitigate this inhomogeneous erosion such as square or rectangular shapes. In that case, the connection length inside the sheath remains constant all along the magnetic field over the electrode (or mirror) surface, so that ionisation is also homogeneous, and thus, the plasma density. Nevertheless, the width of the plasma column still needs to be increased over the sheath layer to allow a constant ion flux to reach the whole mirror surface. This particular issue has no solution as of now, except by considering another plasma source magnetically connected to the mirror.

Data availability statement

The data cannot be made publicly available upon publication because they are not available in a format that is sufficiently accessible or reusable by other researchers. The data that support the findings of this study are available upon reasonable request from the authors.

Acknowledgment

This work has been funded by the Swiss National Science Foundation under agreement No 200021E_189448. This work is supported by the French National Research Agency (ANR) under project SHEAR ANR-19-CE30-033-01. This work was supported by the Swiss State Secretariat for Education, Research and Innovation (SERI) under contract number 22.00424. The authors would like to thank the Swiss Federal Office of Energy, the Swiss Nanoscience Institute and the Federal Office for Education and Science for their Financial support.

Appendix. Experimental setups

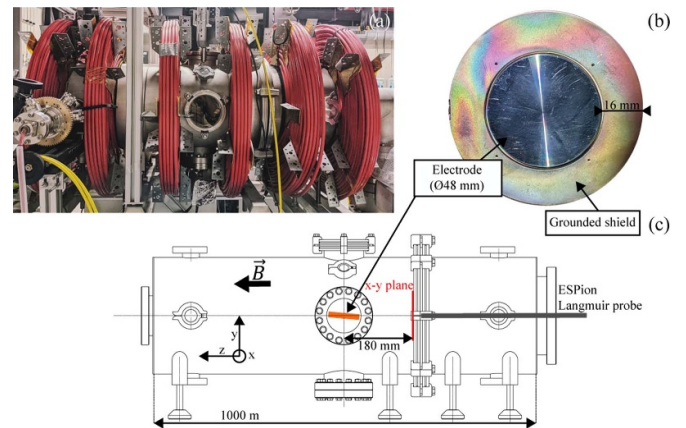


Figure A1. ALINE facility.

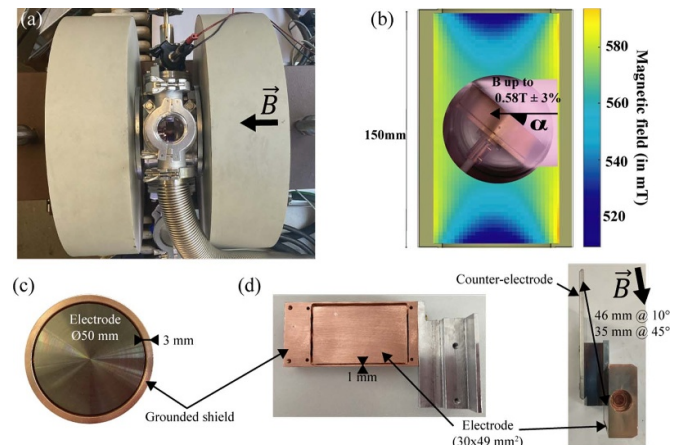


Figure A2. BUMP facility.

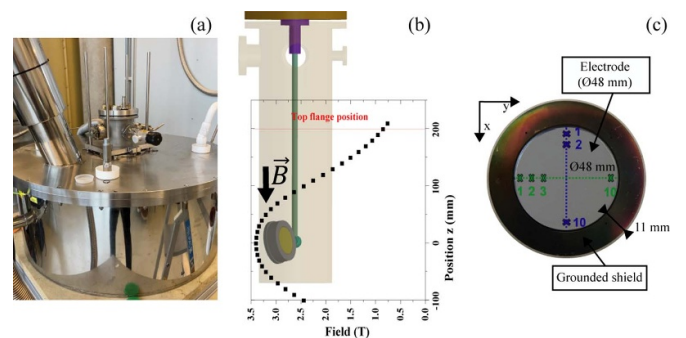


Figure A3. LAMP facility.

ORCID iDs

- Paul Hiret <https://orcid.org/0000-0002-2119-8648>
- Kunal Soni <https://orcid.org/0000-0002-8786-7365>
- Anil Cherukulappurath Mana <https://orcid.org/0000-0001-7455-3984>
- Lucas Moser <https://orcid.org/0000-0003-1766-9942>
- Roland Steiner <https://orcid.org/0000-0002-4350-4132>

Ivo Furno  <https://orcid.org/0000-0001-8348-1716>
 Jérôme Moritz  <https://orcid.org/0000-0002-4593-6270>
 Frédéric Brochard  <https://orcid.org/0000-0002-6578-6046>
 Laurent Marot  <https://orcid.org/0000-0002-1529-9362>
 Ernst Meyer  <https://orcid.org/0000-0001-6385-3412>

References

- [1] Carter M D, Ryan P M, Hoffman D, Lee W S, Buchberger D and Godyak V 2006 *J. Appl. Phys.* **100** 073305
- [2] Müller K P, Heinrich F and Mader H 1989 *Microelectron. Eng.* **10** 55–67
- [3] Lieberman M A and Lichtenberg A J 2005 *Principles of Plasma Discharges and Materials Processing* (Wiley)
- [4] Teh W H et al 2009 *IEEE Int. Interconnect Technology Conf.* pp 53–55
- [5] Wang X, Lee H, Nam S K and Kushner M J 2021 *J. Vac. Sci. Technol. A* **39** 063002
- [6] Brown N P and Walker M L R 2020 *Appl. Sci.* **10** 3775
- [7] Loyan A V and Khaustova A N 2019 Hall thruster erosion *Intechopen*
- [8] Kaganovich I D et al 2020 *Phys. Plasmas* **27** 120601
- [9] Tavant A, Croes V, Lucken R, Lafleur T, Bourdon A and Chabert P 2018 *Plasma Sources Sci. Technol.* **27** 124001
- [10] Petronio F, Tavant A, Charoy T, Alvarez Laguna A, Bourdon A and Chabert P 2021 *Phys. Plasmas* **28** 043504
- [11] Dux R, Bobkov V, Fedorczak N, Iraschko K, Kallenbach A, Neu R, Pütterich T and Rohde V 2007 *J. Nucl. Mater.* **363-365** 112–6
- [12] James A N et al 2013 *Plasma Phys. Control. Fusion* **55** 125010
- [13] Klepper C C et al 2016 *Phys. Scr.* **T167** 014035
- [14] Elias M, Curreli D and Myra J R 2021 *Phys. Plasmas* **28** 052106
- [15] Myra J R and D'Ippolito D A 2015 *Phys. Plasmas* **22** 062507
- [16] Yadav P K et al 2014 *AIP Conf. Proc.* **1591** 890–2
- [17] Cuxart M G, Reyes-Herrera J, Šics I, Goñi A R, Fernandez H M, Carlino V and Pellegrin E 2016 *Appl. Surf. Sci.* **362** 448–58
- [18] Ushakov A et al 2019 *Fusion Eng. Des.* **146** 1559–63
- [19] Walsh M et al 2011 *IEEE/NPSS 24th Symp. on Fusion Engineering* pp 1–8
- [20] Mukhin E E et al 2011 *Nucl. Fusion* **52** 013017
- [21] Marot L, Meyer E, Rubel M, Ivanova D, Widdowson A, Coad J P, Likonen J, Hakola A, Koivuranta S and De Temmerman G 2013 *J. Nucl. Mater.* **438** S1187–91
- [22] Moon S, Petersson P, Rubel M, Fortuna-Zalesna E, Widdowson A, Jachmich S, Litnovsky A and Alves E 2019 *Nucl. Mater. Energy* **19** 59–66
- [23] Litnovsky A et al 2019 *Nucl. Fusion* **59** 066029
- [24] Moser L, Steiner R, Leipold F, Reichle R, Marot L and Meyer E 2015 *J. Nucl. Mater.* **463** 940–3
- [25] Yan R et al 2017 *Nucl. Fusion* **58** 026008
- [26] Soni K, Iyyakkunnel S, Steiner R, Antunes R, Moser L, Bieri O, Marot L and Meyer E 2022 *Nucl. Fusion* **62** 126009
- [27] Chabert P and Braithwaite N 2011 *Physics of Radio-Frequency Plasmas* (Cambridge University Press)
- [28] Chodura R 1982 *Phys. Fluids* **25** 1628
- [29] Devaux S and Manfredi G 2006 *Phys. Plasmas* **13** 083504
- [30] Ahedo E 1997 *Phys. Plasmas* **4** 4419–30
- [31] Kobelev A, Babinov N, Barsukov Y, Chernozumskaya T, Dmitriev A, Mukhin E, Razdobarin A and Smirnov A 2019 *Phys. Plasmas* **26** 013504
- [32] Shigin P et al 2021 *Fusion Eng. Des.* **164** 112162
- [33] Chen F F 2012 *Plasma Sources Sci. Technol.* **21** 055013
- [34] Popov T K, Dimitrova M, Ivanova P, Kovačič J, Gyergyek T, Dejarnac R, Stöckel J, Pedrosa M A, López-Bruna D and Hidalgo C 2016 *Plasma Sources Sci. Technol.* **25** 033001
- [35] Ledig J, Faudot E, Moritz J, Heuraux S, Lemoine N and Usoltceva M 2020 *Plasma Sources Sci. Technol.* **29** 035007
- [36] Ledig J, Faudot E, Moritz J, Heuraux S, Lemoine N and Devaux S 2020 *Contrib. Plasma Phys.* **60** e202000072
- [37] Eren B, Marot L, Litnovsky A, Matveeva M, Steiner R, Emberger V, Wisse M, Mathys D, Covarel G and Meyer E 2011a *Fusion Eng. Des.* **86** 2593–6
- [38] Moser L 2017 *Plasma Cleaning of Diagnostic First Mirrors for the Nuclear Fusion Machine Iter* (University of Basel)
- [39] Eren B, Marot L, Langer M, Steiner R, Wisse M, Mathys D and Meyer E 2011b *Nucl. Fusion* **51** 103025
- [40] Faudot E, Ledig J, Moritz J, Heuraux S, Lemoine N and Devaux S 2019 *Phys. Plasmas* **26** 083503
- [41] Lieberman M A, Lichtenberg A J and Savas S E 1991 *IEEE Trans. Plasma Sci.* **19** 189–96
- [42] Jonkers J, Sande M van de, Sola A, Gamero A and Mullen J van der 2002 *Plasma Sources Sci. Technol.* **12** 30
- [43] Chen F F 2016 *Introduction to Plasma Physics and Controlled Fusion* (Springer International Publishing)
- [44] Gravier E, Brochard F, Bonhomme G, Pierre T and Briangon J L 2004 *Phys. Plasmas* **11** 529–37
- [45] Takeda J, Nezu A and Akatsuka H 2019 *IEEE Trans. Plasma Sci.* **47** 4250–9
- [46] Wu S-M, van de Kruijs R, Zoethout E and Bijkerk F 2009 *J. Appl. Phys.* **106** 054902
- [47] Khaziev R and Curreli D 2015 *Phys. Plasmas* **22** 043503
- [48] Eckstein W, Garcia-Rosales C, Roth J and Ottenberger W 1993 *Sputtering Data* IPP 9/82 Max-Planck-Institut für Plasmaphysik, Garching
- [49] Eckstein W and Preuss R 2003 *J. Nucl. Mater.* **320** 209–13
- [50] Macac E B, Münz W-D and Rodenburg J M 2003 *J. Appl. Phys.* **94** 2829–36
- [51] Wampler W R, Stangeby P C, Watkins J G, Buchenauer D A, Rudakov D L and Wong C P C 2013 *J. Nucl. Mater.* **438** S822–6
- [52] Guterl J, Bykov I, Ding R and Snyder P 2021 *Nucl. Mater. Energy* **27** 100948
- [53] Stangeby P C 2018 *Plasma Phys. Control. Fusion* **60** 044022
- [54] Chrobak C P et al 2018 *Nucl. Fusion* **58** 106019